JACS
JOURNAL OF THE AMERICAN CHEMICAL SOCIETY

Article

pubs.acs.org/JACS

Kinetically Controlled Coassembly of Multichromophoric Peptide Hydrogelators and the Impacts on Energy Transport

Herdeline Ann M. Ardoña,[†,‡] Emily R. Draper,[§] Francesca Citossi,[∥] Matthew Wallace,[⊥] Louise C. Serpell,[∥] Dave J. Adams,*[,§] and John D. Tovar*[,†,‡,#]

[†]Department of Chemistry, Krieger School of Arts and Sciences, [‡]Institute for NanoBioTechnology, and [#]Department of Materials Science and Engineering, Whiting School of Engineering, Johns Hopkins University, 3400 N. Charles Street, Baltimore, Maryland 21218, United States

[§]School of Chemistry, WESTChem, University of Glasgow, Glasgow, G12 8QQ, United Kingdom

[∥]School of Life Sciences, University of Sussex, Falmer, Brighton BN1 9QG, United Kingdom

[⊥]Department of Chemistry, University of Liverpool, Liverpool L69 7ZD, United Kingdom

Supporting Information

ABSTRACT: We report a peptide-based multichromophoric hydrogelator system, wherein π-electron units with different inherent spectral energies are spatially controlled within peptidic 1-D nanostructures to create localized energy gradients in aqueous environments. This is accomplished by mixing different π-conjugated peptides prior to initiating self-assembly through solution acidification. We can vary the kinetics of the assembly and the degree of self-sorting through the choice of the assembly trigger, which changes the kinetics of acidification. The hydrolysis of glucono-δ-lactone (GdL) provides a slow pH drop that allows for stepwise triggering of peptide components into essentially self-sorted nanostructures based on subtle pK_a differences, whereas HCl addition leads to a rapid formation of mixed components within a nanostructure. Using ^{1}H NMR spectroscopy and fiber X-ray diffraction, we determine the conditions and peptide mixtures that favor self-sorting or intimate comixing. Photophysical investigations in the solution phase provide insight into the correlation of energy-transport processes occurring within the assemblies to the structural organization of π-systems.

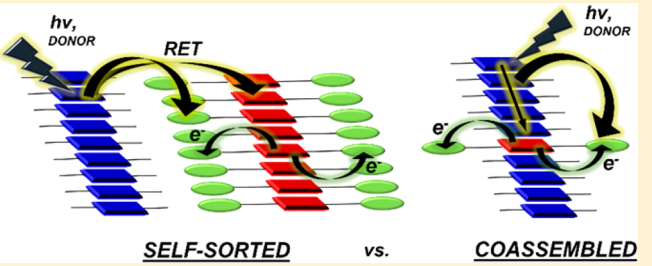

INTRODUCTION

Supramolecular systems can be engineered with dynamic properties as a result of the noncovalent nature of the intermolecular interactions that drive their assembly, so they offer promising materials for mimicking the dynamic nature of physiological environments.[1−3] Multicomponent supramolecular assemblies have been used toward creating artificial light-harvesting complexes, whereby the energy migration from an excited donor to an acceptor occurs within an array of donor−acceptor units.[4−8] There are several examples of multichromophoric assemblies aimed toward applications not only for photosynthetic mimicry but also for excitonic solar cells,[9] light-emitting assemblies,[10−13] and as biophysical molecular rulers.[14] The synthesis details and characterization of energy-transfer events are both equally important for the development of multichromophoric arrays in such applications. For example, Friend, Rowan, and Nolte and co-workers have developed Pt-porphyrin and perylene-bis(dicarboximide) units in polyisocyanopeptides and investigated the sequential energy and electron transfer between the donor and acceptor units.[15] Hodgkiss and Thordarson and co-workers reported a highly efficient multichromophore array based on perylene systems, whereby efficient incoherent energy transfer was reported.[16] Basché and Müllen and co-workers reported terrylene and perylene diimide dyad systems and quantified singlet−singlet annihilation.[17,18] Ajayaghosh and co-workers extensively investigated a library of oligo(*p*-phenylenevinylene) organogelators that are capable of excitation energy transfer between specific donor−acceptor systems.[19−24] A system reported on C_3-symmetric self-sorted units of oligo(*p*-phenylenevinylene) and perylene bisimide was even utilized as a sensing platform for volatile aromatic compounds.[25]

Among the biologically relevant supramolecular structures, peptide-based assemblies appended with π-electron systems, both in solution phase and in xerogels, hold promise for potential applications toward energy-harvesting materials under aqueous conditions[26] as well as solution-processable active layers for device applications such as in field-effect transistors[27−29] and biointerfacing[30−34] applications. Tovar and co-workers previously presented a two-component peptide scaffold bearing oligo(*p*-phenylenevinylene) and quaterthiophene π-electron units that demonstrated excitonic energy transfer.[35] They also demonstrated that quaterthiophene and

Received: April 20, 2017
Published: June 5, 2017

DOI: 10.1021/jacs.7b04006
J. Am. Chem. Soc. XXXX, XXX, XXX−XXX

naphthalenediimide chromophores embedded in the same peptide supported photoinduced electron transfer also under aqueous conditions.[36] Adams and co-workers reported self-sorting among perylene bisimide and stilbene gelators, creating heterojunction arrays with self-sorted fiber networks that led to a photoconductive material.[37] Side-chain functionalization of lysine units with tetraphenylporphyrin and naphthalene diimide was also shown to demonstrate a switch between the H- or J-type of aggregation depending on the protonation state of the porphyrin.[38] In a study that utilized chiral cholesterol moieties, the formation of p-n heterojunctions among self-sorted quaterthiophene- and perylene diimide organogelators was achieved via a heat−cool method, whereby the sequential dissociation and reassembly was governed by the different dissociation constants of each component.[39] We combine three distinct π-electron units (oligo(*p*-phenylenevinylene), quaterthiophene, and naphthalenediimide) within peptidic moieties that form assemblies in aqueous environments under acidic conditions. The combination of photonic donor−acceptor pairs and electron donor−acceptor pairs within one nanostructure enables potentially simultaneous and/or sequential energy- and electron-transfer events and allows for the creation of localized electric fields between the donor and acceptor units that result from charge separation. Moreover, by utilizing different acidification triggers and controlling the kinetics of self-assembly, we aim to control the spatial ordering of the chromophores within the peptidic nanostructure and systematically impact the unique energy-transport processes fostered within these nanostructures.

RESULTS AND DISCUSSION

Design Considerations. We compare the photophysical responses of self-sorted and randomly coassembled binary mixtures of peptides bearing different π-electron systems (Figure 1). To achieve such control over the spatial ordering of the binary peptide mixtures, we modulated the rate of acidification. Although there are several studies conducted on controlling the supramolecular polymerization of multicomponent systems,[40] accurate control over the assembly dynamics and spatial ordering is rarely discussed in the context of engineering the optoelectronic function of a material. A previous report on the nonequilibrium hydrogelation of a quaterthiophene[41] demonstrated that the nanoscale morphologies vary depending on the rate of acid diffusion into the peptide solution: the rapid assembly leads to random but dense matted fiber networks, whereas the relatively slower assembly results in a more homogeneous and anisotropic fiber network.

Here, we use different assembly triggers that lower the pH of the peptide solutions at different rates in order to have control over the kinetics of assembly and the molecular ordering of binary peptide mixtures. Self-sorting was induced via chemical programming, utilizing the difference in the pK_a of the two components as the pH is gradually decreased upon the slow hydrolysis of glucono-δ-lactone (GdL).[42,43] Thus, as the pH slowly decreases, we expect a greater extent of protonation/charge screening for the higher pK_a peptide, triggering it to preferentially assemble first. This should favor the formation of essentially self-sorted structures (Figure 1b). To form the randomly coassembled structures, acid was rapidly added to solutions of essentially dissolved peptide units, whereby global protonation/charge screening of all peptides occurs regardless of the pK_a (Figure 1c). The Asp-Val-Val and Lys-Ala-Ala peptide sequences were chosen for the oligo(*p*-phenylenevinylene)- and quaterthiophene-appended peptides (**OPV3** and **OT4-NDI**), respectively, to establish a difference in the pK_a of each component (see below). The 1,4-distyrylbenzene, an oligo(*p*-phenylenevinylene), serves as an energy donor that upon photoexcitation can funnel the energy to a quaterthiophene unit acceptor. Similarly, the quaterthiophene serves as an excited-state electron donor to the naphthalenediimide in **OT4-NDI**. A control molecule was also synthesized in which the side-chain amine was acylated instead of bearing naphthalenediimide groups (**OT4-Ac**). This control molecule allows us to observe photonic energy-transfer events without the associated electron transfer. We investigate the occurrence of energy-transport processes under aqueous environments in the solution phase and whether the components are self-sorted because of the slow GdL hydrolysis or kinetically coassembled by rapid acidification.

Characterization of Assembly Behavior. The apparent pK_as of the **OPV3** *donor*, the **OT4-NDI** *acceptor*, and the **OT4-Ac** *control acceptor* were observed as pH 6.2, 6.5, and 5.4, respectively (Figure S10). The **OT4-NDI**-containing samples showed buffering regions around pH 12. The gradual titration with aqueous HCl for 1:1 binary mixtures of **OPV3**/ **OT4-NDI** and **OPV3**/ **OT4-Ac** only showed one apparent pK_a rather than a distinct pK_a for each component. To initiate the self-sorting behavior within the two-component peptide hydrogels, 30 mg/mL of GdL was added to the peptide solutions that contained 5 mg/mL of each component. In previous studies with related peptides appended with π-systems, only 5 to 10 mg/mL of GdL was necessary to form hydrogels from 5 mg/mL one-component or binary-peptide gelator solutions.[42,43] The necessary higher GdL concentration for the hydrogelation of the systems reported herein can be possibly attributed to the multiple carboxylates (total of four, two from the backbone termini and two from the aspartic acid side chains, for the **OPV3** donor units) that need to be protonated to favor the self-assembly process. To further monitor the self-assembly

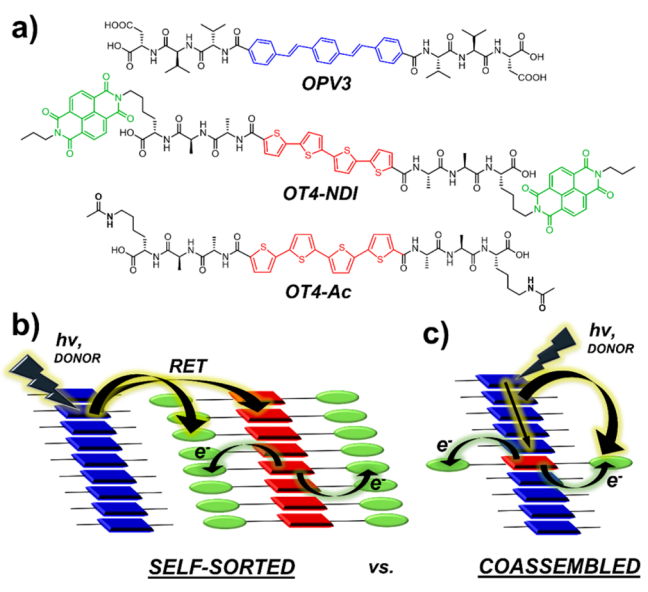

Figure 1. (a) Molecular structures of the peptides studied herein and (b),(c) diagrams of the potential energy (e.g., resonance-energy transfer (RET)) and electron-transfer events occurring within a two-component peptidic nanostructure with three π-electron units for (b) self-sorted and (c) randomly coassembled systems.

DOI: 10.1021/jacs.7b04006
J. Am. Chem. Soc. XXXX, XXX, XXX−XXX

process with GdL, we followed the disappearance of ^{1}H NMR peaks corresponding to the assembly of each gelator component together with the in situ measurement of pH.[44] The assembly is correlated to the disappearance of unique NMR peaks of each component over time, and the results showed a sequential assembly for the 1:1 **OPV3** and **OT4-Ac** mixture (Figure 2a), whereby **OPV3** assembles first. Alternatively, the 1:1 **OPV3** and **OT4-NDI** mixture (Figure S11) did not show any peaks for **OT4-NDI** even at the beginning of the measurement (before the addition of GdL), suggesting that the assembly might have already started for this component even at higher pH conditions (ca. pH 8). This observation of assembly formation at higher pH was analogous to a previously reported hydrophobic oligo(*p*-phenylenevinylene) dipeptide, which favors the formation of wormlike micelles.[45] All homoassemblies (one-component samples) and 1:1 mixed assemblies successfully formed self-supporting gels, as confirmed by the rheology measurements (Figure 2b and S14; the storage modulus G' was an order of magnitude larger than the loss modulus G'' at the end of the time-sweep measurements). The storage moduli values for these hydrogels spanned from 0.02 to 2.5 kPa, with the 1:1 **OPV3** and **OT4-NDI** mixed assemblies having the lowest G' values and the 1:1 **OPV3** and **OT4** mixed assemblies with the assemblies having the highest G' values. For the 1:1 **OPV3** and **OT4-NDI** mixed assembled hydrogel (with a total of 10 mg/mL peptide content) the G' is even lower than its individual components at 5 mg/mL, which demonstrates the complex and nonlinear nature of the mechanical properties of two-component supramolecular systems. These mechanical properties were also observed in another related binary system composed of dipeptide components appended with naphthalene units.[46] Considering the apparent pK_a values from the titration experiments and the spectral information from time-resolved NMR measurements, **OT4-NDI** assembles first, followed by **OPV3** and then **OT4-Ac**. The rheology plots show that the **OT4-Ac** forms the hydrogel the fastest, followed by **OPV3** and then **OT4-NDI** (Figure S14). Correlating the ^{1}H NMR results, which probe molecular-aggregation events, to the time frame of gelation observed from rheological measurements, it is observed that the aggregation time does not coincide with the amount of time required to observe the inflection points for G' and G'' plots for this peptidic system. These plots suggest that for this material and the conditions imposed upon assembly the kinetics of aggregation of the individual components do not directly correlate to the rate at which the fibrillar network reaches the critical fiber-network density to form a hydrogel. Furthermore, because the fiber network density is linked to the bulk mechanical property of hydrogels, there is also no direct correlation that can be made between the kinetics of assembly formation and hydrogel stiffness for these systems.

Further monitoring of the GdL hydrolysis-triggered gelation process via fiber X-ray diffraction supports the occurrence of self-sorting based on the presence of distinct signals from the individual components (Figure 3). No diffraction pattern was observed for **OT4-NDI** as a result of the difficulty in aligning the weaker gels (G' < 100 Pa) between the capillaries used for the measurements. The persistence of diffraction signals from pure **OPV3** (9.3 Å and 4.61/4.7 Å, Figure 3a) and pure **OT4-Ac** (5.6 and 4.61 Å, Figure 3b) in the mixed-peptide assemblies prepared with GdL indicates the self-sorted nature of the nanostructures (Figure 3c,d).[42] From these characterization techniques, we determined the chronology of aggregation and the onset of peptide gelation, and we established that self-sorting occurs when hydrogels are prepared with GdL for both **OPV3**/**OT4-Ac** and **OPV3**/**OT4-NDI** systems.

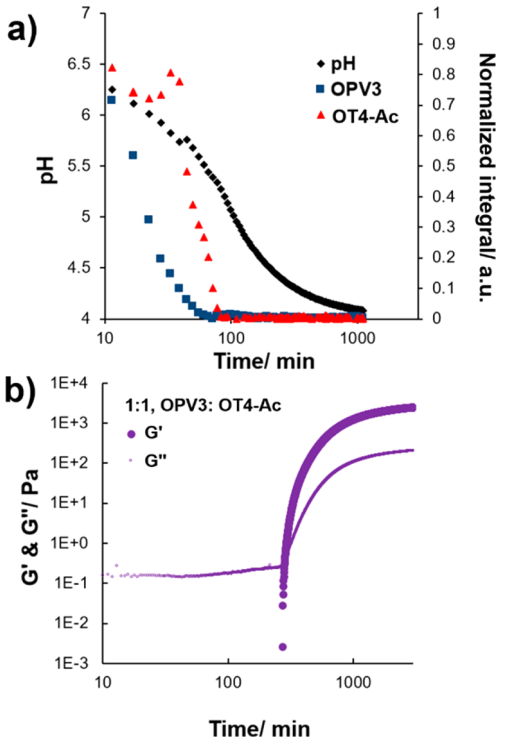

Figure 2. Monitoring of peptide assembly and hydrogel formation for 1:1 **OPV3** and **OT4-Ac** solutions prepared with 30 mg/mL GdL via (a) ^{1}H NMR and (b) rheology (G' = solid circles; G'' = smaller circles). Each peptide component is at 5 mg/mL (total of 10 mg/mL peptides for the 1:1 mixed sample).

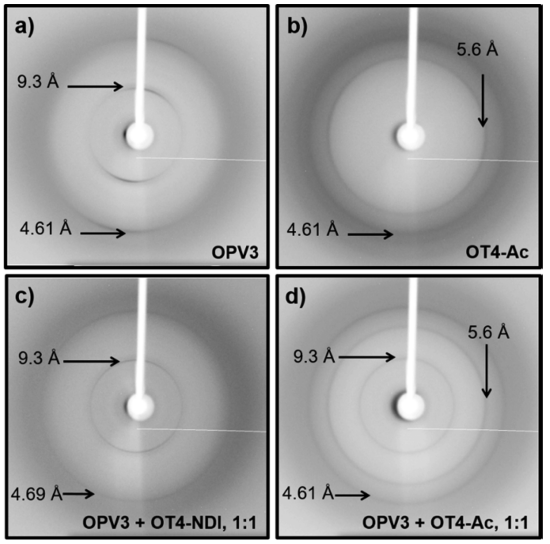

Figure 3. Fiber X-ray diffraction data for hydrogels prepared with 30 mg/mL GdL, composed of one peptide component ((a) **OPV3** only; (b) **OT4-Ac** only) and two peptide components ((c) **OPV3**/**OT4-NDI**; (d) **OPV3**/**OT4-Ac**; both 1:1). Each peptide component is at 5 mg/mL (total of 10 mg/mL peptides for the 1:1 mixed samples).

DOI: 10.1021/jacs.7b04006
J. Am. Chem. Soc. XXXX, XXX, XXX−XXX

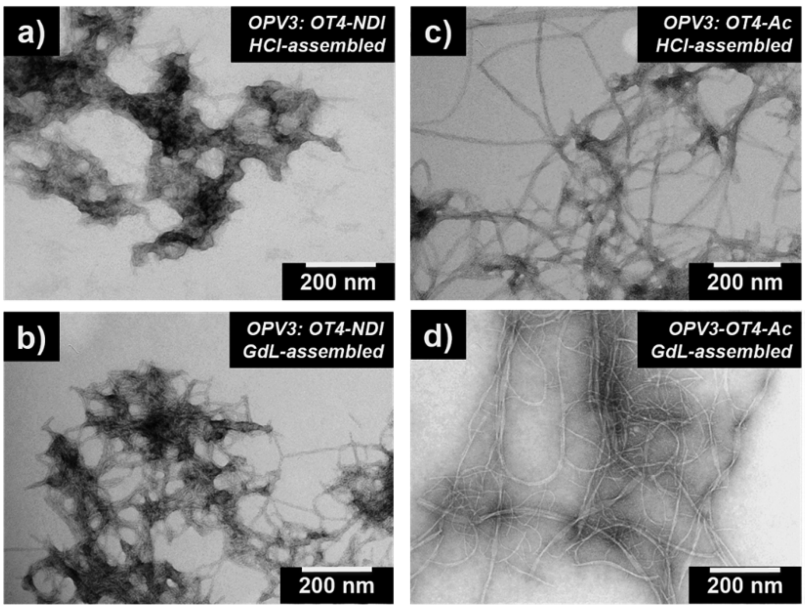

Figure 4. TEM images of 1:1 mixed assemblies (3 μM peptide concentration for each component) of **OPV3** with (a),(b) **OT4-NDI** or (c),(d) **OT4-Ac** (1:1) assembled via (a),(c) HCl addition and (b),(d) GdL (10 mg/mL) hydrolysis.

TEM was used to visualize the nanostructures resulting from GdL or HCl addition (ca. 3 μM peptide concentration for each component). Under such dilute conditions, 10 mg/mL GdL was enough to observe nanostructure formation. For the **OPV3** and **OT4-Ac** homoassemblies (Figure S15), both methods of triggering assembly resulted in the same type of 1-D morphologies. For the **OT4-NDI** peptides, rapid acidification with HCl shows some evidence of micellar-shaped random aggregates, whereas the addition of GdL results in structures with 1-D morphology coexisting with these micellar structures. The predominantly micellar nature of nanostructures formed by **OT4-NDI** with GdL and HCl further supports the formation of relatively weaker gels than for the other peptides because such low-aspect-ratio structures generally have a lower propensity to form cross-links among the nanostructures. For the **OPV3** and **OT4-NDI** mixed assemblies, both the rapid acidification with HCl and the addition of GdL result in the formation of micellar structures along with 1-D nanostructures (Figure 4a,b). In contrast, the mixed assemblies of **OPV3** and **OT4-Ac** (Figure 4c,d) both show 1-D nanostructures with high aspect ratios.

Photophysical Characterization. We utilized the π-electron units embedded in the peptidic moieties, each with unique spectroscopic signatures, as reporters to obtain more information about the spatial organization occurring within the nanostructures under HCl or GdL assembly conditions. The steady-state photophysical spectra of the homoassemblies and mixed assemblies triggered to assemble via HCl and GdL in the aqueous solution phase (Figures 5, 6, and S16) consistently showed trends for H-like aggregation. Namely, this included blue-shifted, quenched absorption and red-shifted, quenched photoluminescence (PL) of the assembled samples as compared to their molecularly dissolved states. The recorded spectra from these aqueous solutions should be treated as ensemble averages of the response from polydisperse solutions of peptide assemblies. The spectra for HCl-triggered solutions were recorded immediately after acidification (i.e., within 1 h) whereas the GdL-triggered samples were measured at 20 h to allow enough time for the lactone to hydrolyze and produce

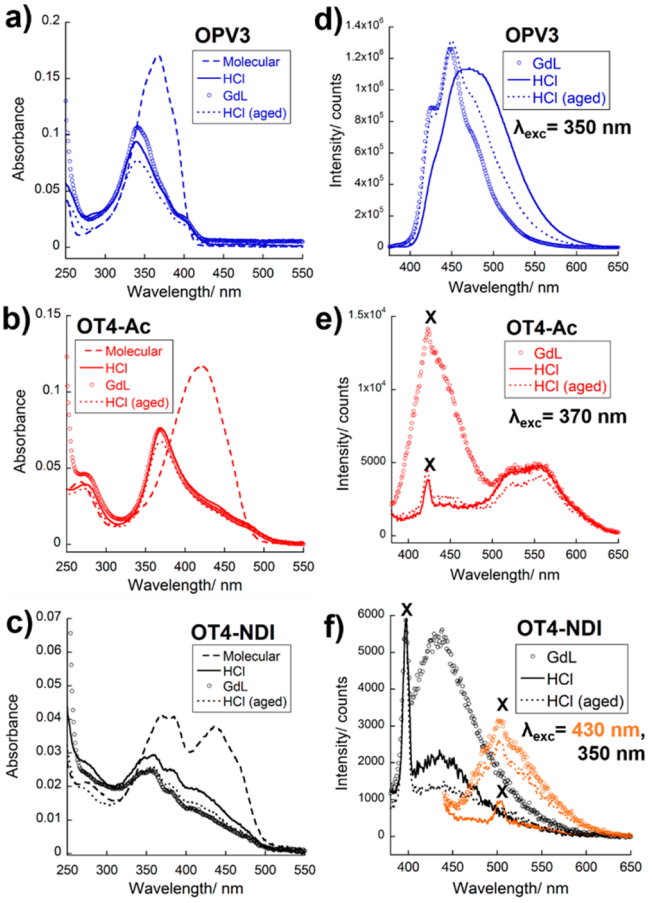

Figure 5. Solution-phase UV–vis absorption (a–c) and steady-state emission (d–f) spectra for GdL- (10 mg/mL) or HCl-assembled peptide homoassemblies of (a) **OPV3** (blue), (b) **OT4-Ac** (red), and (c) **OT4-NDI** (black); solutions measured under different conditions: molecularly dissolved samples (---), (a),(d) with GdL (empty circles), (b),(e) with HCl (—), and (c),(f) with HCl, aged (...); [**peptide**] = 3 μM; X= Raman scatter of water.

DOI: 10.1021/jacs.7b04006
J. Am. Chem. Soc. XXXX, XXX, XXX–XXX

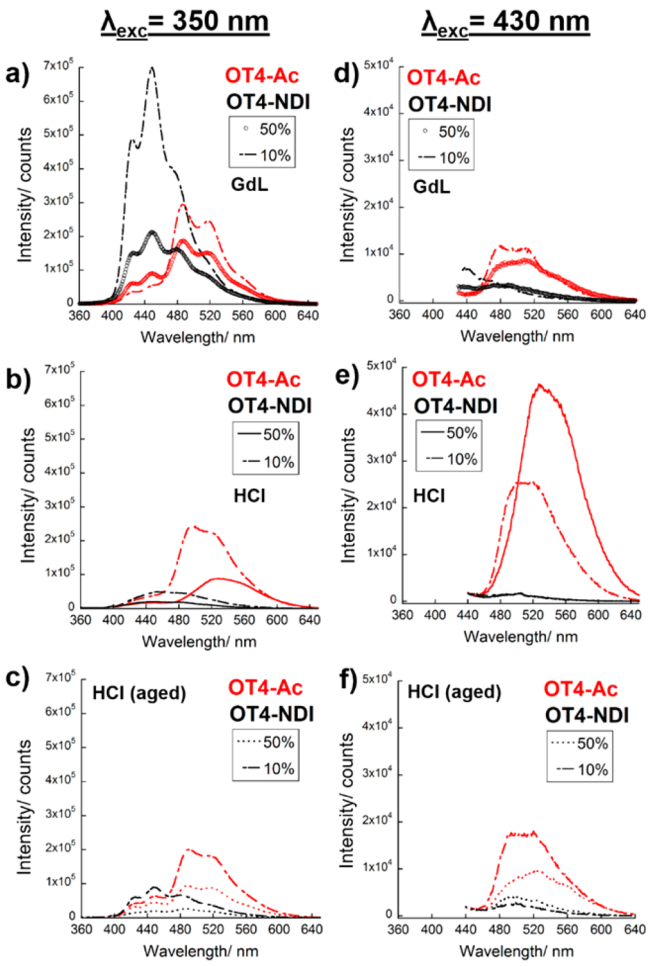

Figure 6. Solution-phase steady-state PL spectra for mixed peptide structures of **OPV3** with **OT4-Ac** (red) and with **OT4-NDI** (black) prepared with GdL (10 mg/mL) or HCl, measured under different conditions: (a–c) λ_{exc}= 350 nm; (d–f) λ_{exc}= 430 nm; (a) with GdL (empty circles), (b) with HCl (—), and (c) with HCl, aged (...); [**OPV3**] = 3 μM.

enough acid to achieve the same pH as the HCl-triggered solutions. The HCl-assembled samples were then aged for the same amount of time that the GdL was allowed to hydrolyze, after which the absorption and PL spectra were then remeasured. For this multichromophoric system, the spectral overlap between the emission of the oligo(*p*-phenylenevinylene) donor with the absorption of quaterthiophene or naphthalenediimide acceptors encourages energy transfer via exciton migration or resonance-energy transfer (RET) from the donor to these acceptors, with a better spectral overlap with quaterthiophene. For quaterthiophene and naphthalenediimide, their relative HOMO and LUMO levels encourage excited-state electron transfer and inhibit energy transfer upon photoexcitation as previously reported.[36] As a point of reference, the spectral properties of the homoassemblies prepared via GdL- and HCl-mediated assembly showed no apparent differences in the maximum absorption peaks except for some slight intensity variations (Figure 5a–c). The aged HCl-assembled samples more closely resemble the absorption spectra of the GdL-assembled samples, suggesting the presence of kinetically trapped structures formed by rapid acidification. They also suggest the dynamic nature of these assemblies, which allow some extent of reorganization over time.

The PL spectra for the homoassemblies of **OPV3**, **OT4-Ac**, and **OT4-NDI** all showed different features when assembled via GdL hydrolysis or via rapid HCl addition (Figure 5d–f). The HCl-assembled **OPV3** shows a broad emission with λ_{max} = 470 nm, whereas the aged HCl- and GdL-triggered assemblies show blue-shifted peaks with more resolved vibronic bands at 420, 440, and 470 nm, suggesting a different packing pattern than for the initially trapped HCl assemblies. These bands can be assigned to strong exciton coupling and are consistent with those that we have observed for the thermally annealed structures of other **OPV3** tetrapeptides.[35] These results support that the slower hydrolysis of GdL could be achieving a more thermodynamically favored structure that is accessed after a dynamic rearrangement due to heating or aging of the kinetically trapped structures formed after rapid acidification.[47−49] For **OT4-Ac** and **OT4-NDI** excited at 370 and 350 nm (maximum absorption for assembled **OT4-Ac** and **OPV3**, respectively; naphthalenediimide has minimal absorption at 350 nm), the PL peak of the aged HCl-assembled solutions does not vary from the early time-point measurements. The **OT4-NDI** peptide excited at 350 nm shows an emission profile that corresponds to minimal PL contributions from naphthalenediimide. However, for excitation at 430 nm, which corresponds to the quaterthiophene component of **OT4-NDI**, the GdL-assembled and aged HCl samples both show a very weak 510 nm peak similar to the maximum PL peak for a monomeric quaterthiophene peptide. The aged HCl-assembled sample shows a completely quenched spectrum (430 nm excitation), with the Raman peak from water at 500 nm as the only apparent feature. Figure 5e,f show signals with very weak intensities and apparent Raman scattering peaks for water. The weak signals are expected from the weakly fluorescent quaterthiophene assemblies but can also be a consequence of the electron transfer from quaterthiophene to naphthalenediimide units.

For the mixed assemblies, analogous to the observations in our previous study for an oligo(*p*-phenylenevinylene)-based donor–acceptor system,[50] it is expected that the photophysical behavior will reflect the spatial organization of the π-electron units, whether it is self-sorted via GdL-triggered assembly or randomly coassembled via HCl-triggered assembly. The absorption profiles are dominated by the **OPV3** signals, which have the highest extinction coefficient among the three chromophores studied, even at 50 mol % of the acceptor units (Figure S16). At 10 and 50 mol %, higher-intensity shoulders at 450 nm are more evident for the HCl-assembled than for the GdL-assembled comixtures. For the PL spectra of mixed assemblies, the samples were excited at 350 nm (where oligo(*p*-phenylenevinylene) has the strongest absorption among the three chromophores) and at 430 nm (where only the quaterthiophene component absorbs). The 10 and 50 mol % **OT4-Ac** in **OPV3** and **OT4-NDI** in **OPV3** are compared under different assembly conditions. In all cases, the PL peak intensities of these mixed-peptide solutions under acidic conditions are lower than that of the **OPV3** homoassemblies as shown in Figure 5d. The 10 and 50 mol % **OT4-Ac** in **OPV3** GdL self-sorted assemblies excited at 350 nm (Figure 6a) both show quenched emission peaks in the **OPV3** region with bimodal peaks around 490 and 520 nm resembling assembled oligothiophene emission in more hydrophobic environments,[51−54] demonstrating some extent of energy transfer. The self-sorted **OT4-NDI** and **OPV3** GdL-assembled samples showed less **OPV3** peak quenching than did the **OT4-Ac** and

DOI: 10.1021/jacs.7b04006
J. Am. Chem. Soc. XXXX, XXX, XXX−XXX

OPV3 self-sorted assemblies but maintained the **OPV3** vibronic progression. The HCl-assembled samples (Figure 6b) showed a similar trend for quaterthiophene PL signatures but with less-resolved spectral features. Compared to the GdL-assembled samples, the **OPV3** emission region was completely quenched, and the peak was further red-shifted to 540 nm at 50 mol %, showing a higher efficiency of energy transfer, which is expected from a more intimate comixing for HCl-assembled samples. Upon aging (Figure 6c), the HCl-assembled samples show more vibronic features in the **OPV3** region but are still more quenched than the self-sorted assemblies prepared with GdL. Furthermore, comparing the **OT4-Ac** and **OT4-NDI** coassemblies with **OPV3** prepared with HCl, the intensities (i.e., relative quantum yields) of the **OT4-NDI** coassemblies are much lower than those of the **OT4-Ac** coassemblies with **OPV3**, verifying the complete energy funneling from oligo(*p*-phenylenevinylene) to quaterthiophene, to relatively spectrally dark naphthalenediimide in the **OT4-NDI/OPV3** coassemblies. This is indicative that energy transfer is still more efficient in the aged HCl-assembled samples than in the GdL-assembled samples, showing that the reorganization that occurs in the kinetically trapped structures formed upon rapid acidification does not achieve the complete self-sorting that is induced with GdL hydrolysis.

For the mixed assemblies excited at 430 nm (Figure 6d–f), the emission spectra provide information on any energy-transfer events that occur from quaterthiophene. The PL signals for self-sorted **OT4-Ac** and **OPV3** mixed assemblies prepared with GdL coincide with the emission of assembled **OT4-Ac** homoassemblies, which is consistent with self-sorting. For the HCl-assemblies at 50 mol % **OT4-Ac**, the PL spectrum has a maximum emission peak at ca. 540 nm, which coincides with what was previously reported for quaterthiophene peptides,[29,51] whereas the maximum emission peak for 10 mol % **OT4-Ac** at 510 nm is reminiscent of molecularly dissolved samples prepared under basic conditions. At 10 mol %, where **OT4-Ac** is a minority component in the comixture, the similarity of the PL profile to molecularly dissolved samples suggests that most of the **OT4-Ac** units are isolated within 90 mol % **OPV3** 1-D nanostructures. Upon aging of the HCl-assembled samples, the 50 mol % **OT4-Ac** sample showed a similar bimodal peak to that observed in GdL-assembled samples, whereas the 10 mol % sample showed a broader quenched peak. For the **OT4-NDI/ OPV3** HCl-triggered mixed assemblies, the quaterthiophene PL region showed a significant quenching as compared to the **OT4-Ac** and **OPV3** samples, which are prepared with the same concentration of quaterthiophene units.

These results support the idea that the selective electron transfer from quaterthiophene to naphthalenediimide upon excitation at 430 nm efficiently occurs without preference as to the assembly method used. For the mixed assemblies excited at 350 nm, the steady-state emission behavior supports that the sequential and/or concerted energy/electron transfer events from **OPV3** to **OT4-Ac/OT4-NDI** occur more efficiently when the components are randomly mixed (prepared with HCl) than self-sorted (prepared with GdL). These data demonstrate the dependence of the photophysical behavior on the choice of assembly trigger (GdL vs HCl) for solution-phase assembly. Hence, the spatial organization of the chromophores within the peptide nanostructures coincides with the structural information obtained for these samples in the gel phase via ^{1}H NMR and fiber XRD (Figures 2a and 3).

Circular dichroism (CD) measurements confirm that both the HCl and GdL-assembled peptide nanostructures maintain similar chirality in both pure and mixed assemblies, except for **OT4-NDI** (Figure S17). Low-intensity CD signals were recorded for **OT4-NDI** homoassemblies corresponding to the naphthalenediimide region of absorption but not for quaterthiophene. Bisignate signals within the region of chromophore absorption corresponding to an exciton-coupled Cotton band were observed for all other peptide nanostructures prepared under both assembly conditions, which is indicative of the local chiral environment of the π-systems undergoing exciton coupling. The CD signals within the high-energy region that distinguish the structural motifs for conventional peptides were not observed for GdL-assembled samples because of a high intensity signal from chiral GdL and gluconic acid as well as interference from sample scattering (Figure S18). For the HCl-assembled samples, the broad peak with minima at ∼250 nm corresponds to a red-shifted β-sheet signal, which is correlated to local twisting within individual assembly units.[55,56]

CONCLUSIONS

A two-component peptide hydrogelator system with multichromophoric units can be spatially engineered on the basis of the choice of the assembly trigger. The slow hydrolysis of GdL provides access to self-sorted structures if each of the components has a different pK_a. However, rapid addition of HCl to the peptide solutions favors the random comixing of two components within the same nanostructure, which can reorganize upon aging. Both methods of assembly led to the formation of self-supporting hydrogels. ^{1}H NMR spectroscopy and fiber XRD support that self-sorting behavior is induced when GdL is added to the binary peptide mixtures. Correlating the ^{1}H NMR spectra and rheology profiles, aggregation occurs the fastest for **OT4-NDI**, but the fastest gelation was achieved with **OT4-Ac**. Thus, aggregation can start earlier in one component, but the propagation of the supramolecular polymerization leading to entangled networks that can support a hydrogel structure can occur at a different rate. Whether the two components were randomly coassembled or self-sorted, the chirality within the nanostructures was maintained as evidenced by the exciton-coupled CD bands within the region of the peptide-embedded chromophore absorptions. Both randomly coassembled and self-sorted peptide nanostructures showed evidence for energy and electron transfer. Selectively exciting **OPV3** initiates exciton migration and resonance energy transfer, which both occur more efficiently if the chromophores are randomly coassembled within one nanostructure. However, the excited-state electron transfer from quaterthiophene to napthelenediimide does not require any specific comixing. This work provides new insights into the photophysical behavior of multichromophoric peptide assemblies whether the components are self-sorted, which is useful for establishing p-n heterojunctions, or randomly comixed, which is useful for creating photosynthetic mimics that require high energy-transfer efficiency. The observation of multiple energy-transport processes in completely aqueous environments, along with the ability to spatially control the distribution of π-electron units within peptidic nanostructures, is an important step in the continued engineering of functional bioelectronic materials.

DOI: 10.1021/jacs.7b04006
J. Am. Chem. Soc. XXXX, XXX, XXX−XXX

■ ASSOCIATED CONTENT

Supporting Information

The Supporting Information is available free of charge on the ACS Publications website at DOI: 10.1021/jacs.7b04006.

General synthesis procedures and experimental conditions; characterization data for peptides (^{1}H NMR, ESI-MS, HPLC traces); pH titration curves; ^{1}NMR stacked plots and data for monitoring OPV3 and OT4-NDI assembly with GdL; supplementary rheology data, TEM images, UV−vis absorption spectra, and CD spectra (PDF)

■ AUTHOR INFORMATION

Corresponding Authors

*tovar@jhu.edu

*dave.adams@glasgow.ac.uk

ORCID

Herdeline Ann M. Ardoña: 0000-0003-0640-1262

Louise C. Serpell: 0000-0001-9335-7751

Dave J. Adams: 0000-0002-3176-1350

John D. Tovar: 0000-0002-9650-2210

Notes

The authors declare no competing financial interest.

■ ACKNOWLEDGMENTS

We thank Johns Hopkins University and the NSF DMR Biomaterials program (1407493). H.A.M.A. is thankful for the generous support from Howard Hughes Medical Institute (International Student Research Fellowship) and Schlumberger Foundation (Faculty for the Future Fellowship). We also thank the Center for Molecular Biophysics (JHU) where circular dichroism measurements were conducted. The NMR spectrometer used for the aggregation time measurements was funded by the EPSRC (EP/C005643/1 and EP/K039687/1). D.J.A. thanks the EPSRC for a Fellowship, which also funded E.R.D. (EP/L021978/1). M.W. thanks Unilever for a Case Award and the EPSRC for funding a DTA. We thank Dr. Laura L. E. Mears for the discussions regarding the structural characterizations of these peptide nanomaterials and for her insightful comments on the manuscript. We dedicate this paper to Professor Samuel I. Stupp (Northwestern University) in recognition of his 40 years of leadership in self-assembling materials.

■ REFERENCES

(1) Aida, T.; Meijer, E. W.; Stupp, S. I. *Science* **2012**, *335* (6070), 813−817.

(2) Webber, M. J.; Appel, E. A.; Meijer, E. W.; Langer, R. *Nat. Mater.* **2015**, *15* (1), 13−26.

(3) Tovar, J. D. *Acc. Chem. Res.* **2013**, *46* (7), 1527−1537.

(4) Jenkins, R. D.; Andrews, D. L. *J. Chem. Phys.* **2003**, *118* (8), 3470−3479.

(5) Kelley, R. F.; Shin, W. S.; Rybtchinski, B.; Sinks, L. E.; Wasielewski, M. R. *J. Am. Chem. Soc.* **2007**, *129* (11), 3173−3181.

(6) Peng, H.-Q.; Niu, L.-Y.; Chen, Y.-Z.; Wu, L.-Z.; Tung, C.-H.; Yang, Q.-Z. *Chem. Rev.* **2015**, *115* (15), 7502−7542.

(7) Ahrens, M. J.; Sinks, L. E.; Rybtchinski, B.; Liu, W.; Jones, B. A.; Giaimo, J. M.; Gusev, A. V.; Goshe, A. J.; Tiede, D. M.; Wasielewski, M. R. *J. Am. Chem. Soc.* **2004**, *126* (26), 8284−8294.

(8) Ziessel, R.; Ulrich, G.; Haefele, A.; Harriman, A. *J. Am. Chem. Soc.* **2013**, *135* (30), 11330−11344.

(9) Gust, D.; Moore, T. A.; Moore, A. L. *Acc. Chem. Res.* **2009**, *42* (12), 1890−1898.

(10) Praveen, V. K.; Ranjith, C.; Armaroli, N. *Angew. Chem., Int. Ed.* **2014**, *53* (2), 365−368.

(11) Vijayakumar, C.; Praveen, V. K.; Ajayaghosh, A. *Adv. Mater.* **2009**, *21* (20), 2059−2063.

(12) Abbel, R.; van der Weegen, R.; Pisula, W.; Surin, M.; Leclère, P.; Lazzaroni, R.; Meijer, E. W.; Schenning, A. P. H. J. *Chem. - Eur. J.* **2009**, *15* (38), 9737−9746.

(13) Giansante, C.; Schafer, C.; Raffy, G.; Del Guerzo, A. *J. Phys. Chem. C* **2012**, *116* (41), 21706−21716.

(14) Sapsford, K. E.; Berti, L.; Medintz, I. L. *Angew. Chem., Int. Ed.* **2006**, *45* (28), 4562−4589.

(15) Huang, Y.-S.; Yang, X.; Schwartz, E.; Lu, L. P.; Albert-Seifried, S.; Finlayson, C. E.; Koepf, M.; Kitto, H. J.; Ulgut, B.; Otten, M. B. J.; Cornelissen, J. J. L. M.; Nolte, R. J. M.; Rowan, A. E.; Friend, R. H. *J. Phys. Chem. B* **2011**, *115* (7), 1590−1600.

(16) Webb, J. E. A.; Chen, K.; Prasad, S. K. K.; Wojciechowski, J. P.; Falber, A.; Thordarson, P.; Hodgkiss, J. M. *Phys. Chem. Chem. Phys.* **2016**, *18* (3), 1712−1719.

(17) Fuckel, B.; Hinze, G.; Nolde, F.; Müllen, K.; Basché, T. *J. Phys. Chem. A* **2010**, *114* (29), 7671−7676.

(18) Stappert, S.; Li, C.; Müllen, K.; Basché, T. *Chem. Mater.* **2016**, *28* (3), 906−914.

(19) Ghosh, S.; Praveen, V. K.; Ajayaghosh, A. *Annu. Rev. Mater. Res.* **2016**, *46* (1), 235−262.

(20) Praveen, V. K.; Ranjith, C.; Bandini, E.; Ajayaghosh, A.; Armaroli, N. *Chem. Soc. Rev.* **2014**, *43* (12), 4222−4242.

(21) Babu, S. S.; Praveen, V. K.; Ajayaghosh, A. *Chem. Rev.* **2014**, *114* (4), 1973−2129.

(22) Ajayaghosh, A.; Praveen, V. K.; Vijayakumar, C.; George, S. J. *Angew. Chem., Int. Ed.* **2007**, *46* (33), 6260−6265.

(23) Ajayaghosh, A.; Praveen, V. K.; Vijayakumar, C. *Chem. Soc. Rev.* **2008**, *37* (1), 109−122.

(24) Vijayakumar, C.; Praveen, V. K.; Kartha, K. K.; Ajayaghosh, A. *Phys. Chem. Chem. Phys.* **2011**, *13* (11), 4942−4949.

(25) Sandeep, A.; Praveen, V. K.; Kartha, K. K.; Karunakaran, V.; Ajayaghosh, A. *Chem. Sci.* **2016**, *7* (7), 4460−4467.

(26) Krieg, E.; Bastings, M. M. C.; Besenius, P.; Rybtchinski, B. *Chem. Rev.* **2016**, *116* (4), 2414−2477.

(27) Sanders, A. M.; Dawidczyk, T. J.; Katz, H. E.; Tovar, J. D. *ACS Macro Lett.* **2012**, *1* (11), 1326−1329.

(28) Besar, K.; Ardoña, H. A. M.; Tovar, J. D.; Katz, H. E. *ACS Nano* **2015**, *9* (12), 12401−12409.

(29) Wall, B. D.; Diegelmann, S. R.; Zhang, S.; Dawidczyk, T. J.; Wilson, W. L.; Katz, H. E.; Mao, H.-Q.; Tovar, J. D. *Adv. Mater.* **2011**, *23* (43), 5009−5014.

(30) Liyanage, W.; Ardoña, H. A. M.; Mao, H. Q.; Tovar, J. D. *Bioconjugate Chem.* **2017**, *28* (3), 751−759.

(31) Du, X.; Zhou, J.; Shi, J.; Xu, B. *Chem. Rev.* **2015**, *115* (24), 13165−13307.

(32) Boekhoven, J.; Stupp, S. I. *Adv. Mater.* **2014**, *26* (11), 1642−1659.

(33) Arslan, E.; Garip, I. C.; Gulseren, G.; Tekinay, A. B.; Guler, M. O. *Adv. Healthcare Mater.* **2014**, *3* (9), 1357−1376.

(34) Loo, Y.; Goktas, M.; Tekinay, A. B.; Guler, M. O.; Hauser, C. A. E.; Mitraki, A. *Adv. Healthcare Mater.* **2015**, *4* (16), 2557−2586.

(35) Ardoña, H. A. M.; Tovar, J. D. *Chem. Sci.* **2015**, *6* (2), 1474−1484.

(36) Sanders, A. M.; Magnanelli, T. J.; Bragg, A. E.; Tovar, J. D. *J. Am. Chem. Soc.* **2016**, *138* (10), 3362−3370.

(37) Draper, E. R.; Lee, J. R.; Wallace, M.; Jäckel, F.; Cowan, A. J.; Adams, D. J. *Chem. Sci.* **2016**, *7* (10), 6499−6505.

(38) Nakayama, T.; Tashiro, K.; Takei, T.; Yamamoto, Y. *Chem. Lett.* **2017**, *46* (4), 423−425.

(39) Sugiyasu, K.; Kawano, S.-i.; Fujita, N.; Shinkai, S. *Chem. Mater.* **2008**, *20* (9), 2863−2865.

(40) Besenius, P. *J. Polym. Sci., Part A: Polym. Chem.* **2017**, *55* (1), 34−78.

DOI: 10.1021/jacs.7b04006
J. Am. Chem. Soc. XXXX, XXX, XXX−XXX

(41) Li, B.; Li, S.; Zhou, Y.; Ardoña, H. A. M.; Valverde, L. R.; Wilson, W. L.; Tovar, J. D.; Schroeder, C. M. *ACS Appl. Mater. Interfaces* **2017**, *9* (4), 3977−3984.
(42) Morris, K. L.; Chen, L.; Raeburn, J.; Sellick, O. R.; Cotanda, P.; Paul, A.; Griffiths, P. C.; King, S. M.; O'Reilly, R. K.; Serpell, L. C.; Adams, D. J. *Nat. Commun.* **2013**, *4*, 1−6.
(43) Draper, E. R.; Eden, E. G. B.; McDonald, T. O.; Adams, D. J. *Nat. Chem.* **2015**, *7* (10), 848−852.
(44) Wallace, M.; Iggo, J. A.; Adams, D. J. *Soft Matter* **2015**, *11* (39), 7739−7747.
(45) Castilla, A. M.; Wallace, M.; Mears, L. L. E.; Draper, E. R.; Doutch, J.; Rogers, S.; Adams, D. J. *Soft Matter* **2016**, *12* (37), 7848−7854.
(46) Draper, E. R.; Wallace, M.; Schweins, R.; Poole, R. J.; Adams, D. J. *Langmuir* **2017**, *33* (9), 2387−2395.
(47) Korevaar, P. A.; Newcomb, C. J.; Meijer, E. W.; Stupp, S. I. *J. Am. Chem. Soc.* **2014**, *136* (24), 8540−8543.
(48) Tantakitti, F.; Boekhoven, J.; Wang, X.; Kazantsev, R. V.; Yu, T.; Li, J.; Zhuang, E.; Zandi, R.; Ortony, J. H.; Newcomb, C. J.; Palmer, L. C.; Shekhawat, G. S.; de la Cruz, M. O.; Schatz, G. C.; Stupp, S. I. *Nat. Mater.* **2016**, *15* (4), 469−476.
(49) Raeburn, J.; Cardoso, A. Z.; Adams, D. J. *Chem. Soc. Rev.* **2013**, *42* (12), 5143−5156.
(50) Ajayaghosh, A.; Vijayakumar, C.; Praveen, V. K.; Babu, S. S.; Varghese, R. *J. Am. Chem. Soc.* **2006**, *128* (22), 7174−7175.
(51) Ardoña, H. A. M.; Besar, K.; Togninalli, M.; Katz, H. E.; Tovar, J. D. *J. Mater. Chem. C* **2015**, *3* (25), 6505−6514.
(52) Pratihar, P.; Ghosh, S.; Stepanenko, V.; Patwardhan, S.; Grozema, F. C.; Siebbeles, L. D. A.; Würthner, F. *Beilstein J. Org. Chem.* **2010**, *6* (1), 1070−1078.
(53) Guo, Z.; Song, Y.; Gong, R.; Mu, Y.; Jiang, Y.; Li, M.; Wan, X. *Supramol. Chem.* **2014**, *26* (5−6), 383−391.
(54) Stone, D. A.; Hsu, L.; Stupp, S. I. *Soft Matter* **2009**, *5* (10), 1990−1993.
(55) Aggeli, A.; Nyrkova, I. A.; Bell, M.; Harding, R.; Carrick, L.; McLeish, T. C. B.; Semenov, A. N.; Boden, N. *Proc. Natl. Acad. Sci. U. S. A.* **2001**, *98* (21), 11857−11862.
(56) Manning, M. C.; Illangasekare, M.; Woody, R. W. *Biophys. Chem.* **1988**, *31* (1−2), 77−86.

DOI: 10.1021/jacs.7b04006
J. Am. Chem. Soc. XXXX, XXX, XXX−XXX